Analyst

Bromide ion-functionalized nanoprobes for sensitive and reliable pH measurement by surface-enhanced Raman spectroscopy

Journal:	*Analyst*
Manuscript ID	AN-ART-09-2019-001699.R2
Article Type:	Paper
Date Submitted by the Author:	24-Oct-2019
Complete List of Authors:	Guo, Huiyuan; Virginia Tech Huang, Qishen; Virginia Tech Leng, Weinan; Virginia Tech, Civil and Environmental Engineering Zhan, Ying; Virginia Tech Behkam, Bahareh; Virginia Tech, Mechanical Engineering Willner, Marjorie; Virginia Polytechnic Institute and State University, Civil and Environmental Engineering Wei, Haoran; Virginia Tech, Civil and Environmental Engineering Marr, Linsey; Virginia Tech, Civil and Environmental Engineering Vikesland, Peter; Virginia Polytechnic Institute and State University, Civil and Environmental Engineering

SCHOLARONE™
Manuscripts

Bromide ion-functionalized nanoprobes for sensitive and reliable pH measurement by surface-enhanced Raman spectroscopy

Huiyuan Guo,[a,b] Qishen Huang,[a,b,c] Weinan Leng,[a,b,c] Ying Zhan,[d] Bahareh Behkam,[d] Marjorie R. Willner,[a,b,c] Haoran Wei,[a,b,c] Linsey C. Marr,[a,b,c] Peter J. Vikesland,[a,b,c,*]

[a]Department of Civil and Environmental Engineering, Virginia Tech, Blacksburg, Virginia;

[b]Virginia Tech Institute for Critical Technology and Applied Science (ICTAS) Sustainable Nanotechnology Center (VTSuN), Blacksburg, Virginia;

[c]Center for the Environmental Implications of Nanotechnology (CEINT), Duke University, Durham, North Carolina;

[d]Department of Mechanical Engineering, Virginia Tech, Blacksburg, Virginia.

[*] Corresponding author

Abstract

4-mercaptopyridine (4-Mpy) is a pH reporter molecule commonly used to functionalize nanoprobes for surface-enhanced Raman spectroscopy (SERS) based pH measurements. However, nanoprobes functionalized by 4-Mpy alone have low pH sensitivity and are subject to interference by halide ions in sample media. To improve nanoprobe pH sensitivity and reliability, we functionalized gold nanoparticles (AuNPs) with both 4-Mpy and bromide ion (Br^-). Br^- electrostatically stabilizes protonated 4-Mpy, thus enabling sensitive SERS detection of the protonation state of 4-Mpy as a function of pH while also reducing variability caused by external halide ions. Through optimization of the functionalization parameters, including suspension pH, [4-Mpy], and [Br^-], the developed nanoprobes enable monitoring of pH from 2.1 to 10 with high SERS activity and minimal interference from halide ions within the sample matrix. As a proof of concept, we were able to track nanoprobe location and image the pH distribution inside individual cancer cells. This study provides a novel way to engineer reliable 4-Mpy-functionalized SERS nanoprobes for the sensitive analysis of spatially localized pH features in halide ion-containing microenvironments.

Introduction

Surface-enhanced Raman spectroscopy (SERS) is a promising technique for chemical and biological analyses. Interest in SERS is rapidly increasing owing to its many advantages, including rapid data collection, high resolution, high sensitivity, low fluorescence interference, and molecular fingerprinting with narrow and differentiable Raman bands.[1–3] These advantages make SERS an ideal option for application in complex chemical and biological environments.

pH is a critical trait that dictates chemical and biological reactions, partitioning, and reactivity in confined microenvironments such as cells[4–7] and aerosol droplets[8,9]. Quantification of pH in confined microenvironments is experimentally challenging because of their inaccessibility to conventional pH probes. To address this issue, a number of nanoprobes have been designed for SERS based pH sensing.[10–15] These nanoprobes are typically functionalized with pH-sensitive reporter molecules. The reporter molecules enable pH measurement because the vibrations of their functional groups and the corresponding SERS peaks vary as a function of the local pH. As a result, the pH in microenvironments can be quantified based on calibration curves that relate SERS spectral pattern changes with pH. The most commonly used pH reporter molecules are aminothiolphenol (ATP),[12,13] 4-mercaptobenzoic acid (4-MBA),[15–17] and 4-mercaptopyridine (4-Mpy)[18–21]. What these chemicals have in common is that they all contain a thiol group that strongly binds to the metal nanoparticle surface and enables surface functionalization. The differences lie in their molecular pH sensitive moieties. ATP exists in different isomers, including 4-ATP and 2-ATP and their pH-sensing ability is based on the protonation/deprotonation of the primary amine (NH_2/NH_3^+). Unfortunately, primary amines are subject to coupling reactions in alkaline solution to produce -N=N- linkages and the formation of dimercaptoazobenzene (DMAB).[22] Such chemical instability may account for the reported decrease in quantification accuracy for pH $\geq$ 6.[12,13] Distinct

from ATP, 4-MBA enables pH measurement through the protonation/deprotonation of the carboxylic acid ($COOH/COO^-$), which has three limitations. First, the carboxylic moiety could be lost due to decarboxylation on plasmonic-active surfaces under certain conditions, such as strong laser intensity.[17] Second, 4-MBA does not induce high SERS enhancements due to its weak capacity to form nanoparticle aggregates and SERS "hotspots".[15] Furthermore, the high pK_a (8.75)[15] of $COOH/COO^-$ makes 4-MBA functionalized particles insensitive at low pH values.[16]

4-Mpy, a pyridine derivative, is chemically stable and exhibits SERS pattern changes in acidic conditions due to the low pK_a (3.0-3.9) of N protonation/deprotonation[23–25] on metal nanoparticle surfaces. A number of research groups have made efforts to develop pH nanoprobes that are functionalized with 4-Mpy.[18–21] However, to date these studies have failed to account for the potential impacts of halide ions on the pH-sensing capacity of the 4-Mpy-functionalized nanoprobes. Prior work has shown that halide ions can alter the pyridine SERS spectrum under acidic conditions.[26–30] As a pyridine derivative, 4-Mpy can be expected to exhibit variations in its SERS spectra in the presence of halide ions that may impact its use as a pH sensing molecule. Therefore, there is a need to determine how the pH sensitivity of 4-Mpy-based nanoprobes is impacted by halide ions and if necessary, to minimize halide ion interference. This is a critical need given that halide ions are ubiquitous in natural and cellular environments.[31,32]

To address the potential impacts of halide ions on 4-Mpy reactivity, we chose to produce probes pre-functionalized with Br^-. Previous studies have shown that halide ions specifically adsorb onto metal surfaces with binding strengths increasing from $F^- < Cl^- < Br^- < I^-$.[33–35] Among these, Cl^-, Br^-, and I^- all form strong covalent bonds (Au-X) with the gold nanoparticle (AuNP) surface[33–35], with both Br^- and I^- having sufficient affinity to the AuNP surface to displace surface ligands (e.g., citrate).[36] Adsorbed I^- is known to etch AuNPs and thus leads to nanoparticle fusion,

while Br^- adsorption has been shown to protect AuNPs from fusing.[36] For these reasons, herein we focused on pre-functionalizing the AuNPs with Br^-.

By integrating Br^- functionalization into our nanoprobe design, we developed an innovative pH nanoprobe with high SERS activity and capacity for sensitive application in acidic samples with minimal halide ion interference. As both 4-Mpy and Br^- can induce AuNP aggregation, we optimized the preparation procedure by adjusting the synthesis pH as well as [4-Mpy] and [Br^-]. Following these efforts, the nanoprobes were successfully applied to measure pH in 4T1 murine mammary carcinoma cells with high stability and accuracy.

Materials and Methods

Materials

Gold chloride trihydrate ($HAuCl_4 \cdot 3H_2O$), sodium citrate tribasic dihydrate ($Na_3Citrate \cdot 2H_2O$), and 4-mercaptopyridine (4-Mpy) were obtained from Sigma-Aldrich. Thiolated poly(ethylene glycol) (HS-PEG; 5 kDa) was obtained from Nanocs. Sodium bromide, L-ascorbic acid, HCl (37%), NaOH, and H_2SO_4 (98%) were acquired from Fisher Scientific.

Synthesis and characterization of the pH nanoprobes

Our experimental design involves AuNP synthesis followed by surface functionalization. A seed-mediated growth approach was used to synthesize AuNPs.[37] Briefly, AuNP seeds were produced by bringing 100 mL of 1 mM $HAuCl_4 \cdot 3H_2O$ to boiling and then adding 15 mL of 1% $Na_3Citrate \cdot 2H_2O$ solution under stirring at 1000 rpm. The mixture was refluxed for 15 min in a distillation flask without water loss. After the mixture cooled, the suspension was filtered through a 0.22 μm nitrocellulose membrane and then stored at 4 °C for future use. These seeds were

characterized via dynamic light scattering (DLS, Zetasizer Nano ZS) and found to have a hydrodynamic diameter of 14.7 ± 0.04 nm.

To prepare larger AuNPs, a protocol by Yuan *et al.*[38] was followed with minor revision. Briefly, 0.25 mM $HAuCl_4 \cdot 3H_2O$ dissolved in 1 mM HCl solution (10 mL) was mixed with 100 µL of the citrate-stabilized seeds at room temperature under stirring at 700 rpm. Then, 50 µL of ascorbic acid (100 mM) was added as the reducing and capping agent. After stirring for 30 s, the reaction was stopped by centrifugation at 3260 × g for 15 min. After removing the supernatant, the synthesized AuNPs were redispersed in nanopure water (10 mL) and stored at 4 °C before use.

To produce pH sensitive particles, we initially modified the AuNP surface by adding 4-Mpy (0.75 µM) to replace the original surface ligand (*i.e.*, ascorbic acid). The suspension pH was adjusted to 9 prior to adding 4-Mpy. The nanoparticles were further functionalized with Br^- (20 mM) to achieve high SERS activity and pH sensitivity. We stabilized the produced particles using HS-PEG (0.01 µM) before centrifuging at 3260 × g for 15 min. Following centrifugation, the nanoprobes were redispersed in 2 mL of nanopure water and stored at 4 °C.

Intracellular pH monitoring

Intracellular pH analysis was performed using murine mammary carcinoma cells (4T1, ATCC CRL-2539). The cells were cultured in Roswell Park Memorial Institute (RPMI)-1640 medium with 10% fetal bovine serum (FBS) at 37 °C with 5% CO_2. When the culture became ≈80% confluent, cells were lifted with 0.25% (w/v) trypsin-0.1% (w/v) EDTA solution and the cell density was estimated using a hemocytometer. A 2 mL suspension of cancer cells at 2.4×10^4 cells/mL were seeded in a 35 mm sterile tissue-treated petri dish. Cells were cultured overnight in an incubator at 37 °C with 5% CO_2. The nanoprobes (200 µL of 2×10^{11} particles/mL) were then added into the petri dish and incubated with the cells for 24 hours. Prior to Raman imaging, the

cells were washed with Dulbecco's phosphate buffered saline (DPBS, pH 7.4) thrice and the petri dish was refilled with cell culture medium. During pH measurement, only cells that were securely attached to the petri dish were selected under the Raman microscope for SERS analysis. To quantify pH within the cancer cells, a calibration curve was generated based on the SERS spectra of nanoprobes in cell culture medium with different pH values. The pH was adjusted to a given value by using H_2SO_4 and NaOH.

After measuring pH by SERS, we used the ReadyProbes® Cell Viability Imaging Kit (Blue/Green) to determine cell viability. The assay was performed by adding two drops each of NucBlue® Live reagent (Hoechst 33342) and NucGreen® Dead reagent to 1 mL of cell growth media and incubating for 15 min. Cell viability was evaluated using fluorescence microscopy (Zeiss Axio Observer Z1). NucBlue® Live reagent, which stains the nuclei of all cells, was detected with a standard DAPI filter (excitation/emission maxima: 360/460 nm). NucGreen® Dead reagent, which stains only the nuclei of dead cells with compromised plasma membranes, was detected with a standard FITC/GFP (green) filter set (excitation/emission maxima: 504/523 nm).

Instrumentation

The synthesized nanoprobes were characterized by multiple techniques. An ultraviolet-visible (UV-Vis) spectrophotometer (Cary 5000, Agilent) was used to measure the UV-Vis absorbance spectra of the suspension in a plastic cuvette with 1-cm light path length. The hydrodynamic diameter and zeta potential were determined by a dynamic light scattering instrument (DLS, Zetasizer Nano ZS). Additionally, transmission electron microscopy (TEM, JEOL 2100 S/TEM) was utilized to observe particle size and morphology. The TEM sample was

prepared by dropping the sample on a lacey-carbon coated copper grid and air drying in a clean laminar flow hood.

SERS spectra were recorded by a Raman spectrometer (Alpha500R, WITec) with a 785-nm laser and a 50× confocal microscope objective. The detection settings involve 300 gr/mm grating and 0.1 s integration time. Three replicates were tested for each sample during method development. For each replicate, 400 spectra, acquired across a 100 × 100 μm^2 area, were averaged to produce an overall spectrum (unless noted otherwise) using Project Five (version 5.0). The detection process was monitored using Control Five (version 5.0). Cancer cells were analyzed using the same settings except the detection area was adjusted according to the cell size.

SERS data analysis

The SERS data was analyzed using MATLAB® 2016b (The Mathworks, USA) to baseline correct the spectra and extract the intensities of the peaks of interest (1572 cm^{-1} and 1606 cm^{-1}). Calibration curves were plotted to demonstrate changes of peak ratios as a function of pH. Based on the calibration curve, we were able to convert peak intensity ratios (I_{1572}/I_{1606}) into pH in each pixel of the SERS maps and thus generate a pH distribution map.

Results and Discussion

pH nanoprobe design and development

Fabrication of pH-sensing nanoprobes involved sequential functionalization of the AuNP surface with 4-Mpy and Br^-. To produce nanoprobes with high SERS signal intensity, we first optimized the 4-Mpy concentration. As shown in Figure S1, the SERS signal intensity increased when the 4-Mpy concentration increased from 0.1 to 0.75 μM and then decreased when the concentration exceeded 0.75 μM. As reported previously, the Raman reporter concentration affects

the SERS signal intensity both due to changes in surface coverage[39] and the NP aggregation state[15,40]. In this study, 0.75 μM 4-Mpy was used for nanoprobe functionalization because it ensured full coverage of 4-Mpy on AuNP surface (132% of geometric surface area, see calculation details in SI) and generated AuNP aggregates (DLS size: 75.9 ± 1 nm) with high SERS activity (Figure S1). The zeta potential of AuNPs changed from -41.6 ± 1.0 mV to -30.7 ± 0.1 mV after incubation with 4-Mpy, indicating the replacement of original surface ligand by 4-Mpy.

The second step in nanoprobe production involved the labelling of 4-Mpy-functionalized AuNPs with Br^-. To increase 4-Mpy sensitivity to low pH range through Br^- electrostatically stabilized protonated 4-Mpy and minimize the interference from halide ions in sample matrices, a Br^- concentration that could ensure sufficient Br^- to cover the AuNP surface is favorable. In order to preselect a concentration that meets this requirement, we first tested the interaction of AuNPs with different concentrations of Br ions prior to 4-Mpy modification. As seen in Figure S2, the SERS peak at 189 cm^{-1}, which represents the Au-Br bond, increased from 10 to 20 mM, and flattened from 20 to 30 mM, indicating that the adsorption of Br^- on AuNPs reached the maximum at 20 mM. Hence, 20 mM Br ions was preselected for further experiments.

With 4-Mpy modification, we found that Br^- caused additional AuNP aggregation, giving rise to larger AuNP aggregates (131.1 ± 0.8 nm) and weaker SERS signals (Figure 1a, pH 5.7). This problem was addressed by adjusting the suspension pH before incubating the AuNP colloids with 4-Mpy and Br^-. Based on the color change of the suspension and the corresponding UV-Vis spectra (Figure 1b), we determined that the extent of AuNP aggregation was negatively associated with solution pH. At higher pH values, the extent of nanoprobe aggregation was lower as confirmed by DLS analysis. The hydrodynamic diameter decreased from 131.1 ± 0.8 to 51.2 ± 0.8 nm when pH increased from 5.7 to 10 (Figure S3).

The SERS activity of the nanoprobes synthesized at different initial pH values was examined and the results showed that the highest SERS signal intensity was measured at pH 9 (Figure 1a). For this reason, pH 9 was used for the synthesis of nanoprobes in all subsequent experiments. pH alters the aggregation state of the AuNPs due to its impact on the AuNP surface charge. Zeta potential measurements indicate that the surface charge of the AuNPs was dependent on the pH used for 4-Mpy functionalization (Figure S4). The zeta potential decreased from -30.7 ± 0.1 to -51.6 ± 0.2 mV when pH increased from 5.7 to 10. The increase in negative charge accounts for the decreased aggregation. 4-Mpy, with a reported surface pK_a of 3.0-3.9,[23–25] is neutral or negatively charged[41] in the pH range of 5.7-10 and the higher the pH, the higher the number of negative charges, which explains the pH-dependent stability of 4-Mpy-functionalized AuNPs.

We examined the impact of [Br^-] on the aggregation of 4-Mpy-functionalized AuNPs and their SERS activity. As indicated by a color change and the UV-Vis absorbance data (Figure 1d), [Br^-] impacts the aggregation state of the synthesized nanoprobes. When [Br^-] was increased from 10 to 30 mM, we observed an increase in the DLS size from 49.2 ± 0.8 to 61.7 ± 0.9 nm (Figure S5). Based on the measured SERS signal intensities, 20 mM Br^- induced the highest SERS activity (Figure 1c). As seen in the UV-Vis spectra in Figure 1d, a secondary plasmon band occurred in the near-infrared region due to the coupling of surface plasmons between aggregated particles[42] and was influenced by [Br^-]. It is a well-known phenomenon that SERS enhancement is maximized when the nanosubstrate plasmon band overlaps with the incident laser wavelength.[43–45] Therefore, the closer the secondary band to the incident laser wavelength, the higher the SERS enhancement. In this study, we used a 785 nm laser. The aggregates induced by 20 mM Br^- exhibited an extinction band at around 770 nm which is closest to 785 nm as compared to those generated by 10 mM or

30 mM (Figure 1d). This explains why SERS intensity with 20 mM Br^- was the higher than that with 30 mM Br^-. Accordingly, 20 mM was adopted as the optimal [Br^-] to synthesize the pH nanoprobes.

In this study, we have found that both 4-Mpy and Br^- contributed to the aggregation of AuNPs. Nanoprobes functionalized at pH 9 by a combination of 0.75 μM 4-Mpy and 20 mM Br^- yields strongest SERS signals. Increasing the concentration of either 4-Mpy or 20 mM Br^- could cause additional aggregation and weaken the nanoprobe performance. It is possible to achieve other combinations by increasing [4-Mpy] and decreasing [Br^-]. However, this will compromise the surface coverage of Br^- on AuNPs. As shown in Figure S2, the adsorption of Br^- on AuNPs reached the maximum at 20 mM. Therefore, we did not make future adjustments of [4-Mpy] and [Br^-].

Characterization of the pH nanoprobes

We designed and developed an innovative pH nanoprobe that was functionalized with both 4-Mpy and Br^-. According to the DLS analysis, the pristine AuNPs used for nanoprobe synthesis have an average hydrodynamic diameter of 36.1 ± 0.3 nm. A typical UV-Vis absorbance peak for spherical AuNPs of this size was observed at 526 nm (Figure 2a). The average physical diameter was 36.4 ± 0.7 nm according to TEM analysis (ImageJ, n=100; Figure 2b, 2c). After functionalization by 4-Mpy, Br^-, and stabilization by PEG, the hydrodynamic diameter increased to 57.2 ± 0.7 nm. The UV-Vis spectrum (Figure 2a) exhibits two bands. The one at 528 nm is derived from the localized surface plasmon resonance (LSPR) of gold nanoparticle monomers; the other peak at ~770 nm is the broad extended plasmon band (EPB) arising from gold nanoparticle aggregates.[46,47] These changes in the UV-Vis spectrum are consistent with the increase in

hydrodynamic diameter and suggest moderate aggregation of the AuNPs induced by surface modification.

Nanoprobe-based sensing takes advantage of the spatial sensitivity enabled by nanoscale probes and the high-resolution spectroscopic fingerprint provided by SERS. The spatial volume that a nanoprobe senses is determined by the laser spot size of the Raman microscope objective. The laser spot size is defined in the lateral ($\delta_{lateral}$) and axial (δ_{axial}) dimensions, which were calculated to be 0.68 μm and 3.2 μm, respectively (details in the SI). Assuming a cylindrical laser spot, the detection volume was determined to be 1.2 μm^3. Such a small volume provides SERS-based pH nanoprobes with higher spatial resolution than traditional pH meters.

Advantages of Br^--assisted pH nanoprobes

One of the major improvements made in this study is the incorporation of Br^- into the fabricated pH-sensing nanoprobes. The nanoprobes were surface modified by Br^- to achieve three aims. The first aim was to improve the sensitivity of the nanoprobes to pH changes. As shown in Figure 3, we compared the SERS response of the nanoprobes with or without Br^- functionalization under different pH conditions. Because the signal intensities varied with pH, we normalized all of the peaks relative to the elastic light scattering peak at 81 cm^{-1} to illuminate spectral pattern changes more clearly.[48] Past studies by our group have shown that this normalization approach, using elastic light scattering as an internal standard, can reduce spatial signal variability caused by heterogeneous SERS "hotspots".[39,48] In this manner, intrinsic changes in the reporter molecule on the AuNP surface are directly reflected within the normalized SERS spectrum.[39,49] Based on the observation that the normalized SERS spectrum for nanoprobes in the absence of Br^- at pH 4.5 was similar to that at pH 1.5 (Figure 3a), we established that without Br^- the nanoprobes were insensitive to the acidic pH change. When the AuNP surface was modified by Br^-, the pH

sensitivity was improved with the spectral pattern significantly altered by the pH decrease from 4.5 to 1.5 (Figure 3b). The normalized signal intensity increased for peaks at 1006 and 1606 cm^{-1} and decreased for peaks at 1091 and 1572 cm^{-1}. The effect of Br^- on the sensitivity of the metal surface ligand to pH changes was previously reported for pyridine,[27,30] the major molecular unit of 4-Mpy. It was found that, in the absence of halide ions, the protonated form of pyridine (i.e., pyridinium) is unstable and readily transforms to pyridine on the silver electrode surface,[26,30] thus making SERS detection of pyridinium challenging. However, when halide ions are present, pyridinium interacts with the halide ions to form pyridinium halide that binds to the Ag electrode surface through the halide ions. This mechanism explains why halide ions are required to enable SERS monitoring of the pH-induced chemical changes of pyridine. A similar process could explain our finding that the SERS signals of 4-Mpy are more sensitive to pH changes when halide ions (e.g., Br^-) coexist with 4-Mpy at the AuNP surface. Accordingly, Br^- labelling is a critical step to enable pH sensitivity of 4-Mpy-based SERS nanoprobes.

The second purpose of Br^- modification is to minimize potential interference by halide ions, such as Cl^- and Br^-, within the analyte media. Cl^- is ubiquitous in environmental and biological matrices, with high concentrations around several hundred millimolar in many samples (e.g., in sea water).[31] Br^- has lower concentrations in most natural ecosystems, except in seawater where the concentration can reach 0.8 mM.[31,32] When the nanoprobes were not pre-labelled by Br^- (Figure 4a, 4b), the SERS spectral shape and peak ratios fluctuated when the analyte matrix contained Cl^- or Br^-. As a result, SERS-based pH measurements are skewed by the presence of halide ions in the sample. In contrast, nanoprobes functionalized by Br^- exhibit stable SERS spectra even in the presence of Cl^- or Br^- in the sample media (Figure 4c, 4d). Modification of the AuNP surface by

Br^- during nanoprobe synthesis enables resistance of the nanoprobes to the halide ion interference and enhances the pH measurement accuracy.

The third function of Br^- modification is enhanced SERS activity. Figure 3c demonstrates that nanoprobes with Br^- labelling have 8× increased SERS intensity relative to those without Br^- labelling. Previous studies have reported three modes of action through which halide ions could affect the SERS response of metal nanoparticles: activation,[50] aggregation,[51,52] and desorption[53]. Activation occurs following the formation of stable surface complexes between the metal surface, halide ions, and the molecular adsorbate. Jeanmaire and Van Duyne observed increased Raman enhancement in the presence of Br^- due to complex formation between the silver surface, Br^-, and pyridine.[54] Aggregation occurs when the halide ion concentration is high enough to create aggregates with SERS "hotspots" that enhance Raman signals.[51,52] Desorption is the replacement of the molecular adsorbate by halide ions on the metal surface. In our work, we observed that the SERS signal of protonated 4-Mpy was stabilized by Br^- on the AuNP surface, indicating the formation of complexes between Au, Br^-, and 4-Mpy. Furthermore, the aggregation of 4-Mpy-functionalized AuNPs induced by Br^- (20 mM) was detected with a hydrodynamic diameter increase from 38.5 ± 0.3 (0 mM Br^-) to 57.2 ± 0.7 nm. In addition, the coverage of 4-Mpy was not significantly altered by Br^- modification (Figure S6), showing that Br^- did not result in the desorption of 4-Mpy. Overall, it is suggested that the activation and aggregation caused by Br^- labelling contributed to the improved SERS activity of the pH nanoprobes in this study.

Nanoprobe stability and pH sensitivity in cell culture medium

To establish the utility of our nanoprobes, we conducted intracellular pH analysis using 4T1 murine mammary carcinoma cells. To ensure the availability of the nanoprobes for cancer cell uptake, the nanoprobes must stay suspended and stable in the culture medium over the incubation

period. We tracked nanoprobe stability in the culture media using DLS. The results indicate that the hydrodynamic diameter of the nanoprobes remained around 60 nm over 24 h (Figure 5a), thus confirming the stability of our pH nanoprobes and their availability for cell internalization.

To quantify pH in 4T1 breast cancer cells, a calibration curve showing the relationship between the nanoprobe SERS signal and the sample pH was produced. For that purpose, we first measured cell culture media with pH values ranging from 2.1 to 10 using the developed nanoprobes, and then recorded the corresponding SERS spectra. The peak assignments within the SERS spectra are tabulated in Table S1. Among them, the two peaks at 1006 and 1606 cm^{-1} were chosen as pH reporter bands because they are associated with the protonation and deprotonation of N in 4-Mpy.[55,56] A pH calibration curve was obtained based on the intensity ratio of the two peaks (I_{1572}/I_{1606}) and the culture medium pH. As shown in Figure 5b, the relationship is well fit by a polynomial expression (R^2 = 0.992). Due to their high stablity and pH sensitivity, the nanoprobes developed herein can feasibly measure a wider pH range (2.1-10) than previous pH nanoprobes reported in the literature.[15,16,18–21]

Intracellular pH monitoring in cancer cells

To evaluate the efficacy of our nanoprobes for pH determination in confined microenvironments, the 4T1 murine mammary carcinoma cells was selected as a biological example. 4T1 is a commonly used animal model for human breast cancer.[57,58] Before intracellular pH tracking and imaging by SERS, the nanoprobes were first incubated with 4T1 cancer cells in the culture medium for 24 h to enable nanoprobe internalization. After incubation, the cancer cells were washed by DPBS 3× prior to SERS imaging. To pinpoint the locations of the nanoprobes, the Raman band at 1572 cm^{-1} from 4-Mpy was selected as a marker to create the nanoprobe distribution map. As shown in Figure 6a and 6b, the nanoprobe signal was detected where cancer

cells existed and the optical image of cancer cells matched the distribution map of nanoprobes, thus suggesting that the nanoprobes were co-located with the cancer cells. We demonstrated cellular internalization of the nanoprobes through depth mapping (Figure 6d). The nanoprobe signals were detected across 0-27 μm, which is in agreement with the cancer cell dimension, suggesting that nanoprobes have been successfully taken up by cancer cells. Moreover, maps collected near the upper surface of a cancer cell showed no nanoprobe signals, indicating that the nanoprobes were not attached to the cell surface. It has been reported in the literature that nanoparticles could enter 4T1 breast cancer cells through endocytosis.[59] Our data demonstrate that our nanoprobes were successfully internalized by the 4T1 breast cancer cells and could be used to measure pH inside cancer cells. Meanwhile, the performed cell viability test (Figure S7) shows that 99.6% (272 cells) of cells were alive after nanoprobe internalization and SERS analysis, indicating that the cell viability was not significantly compromised by the nanoprobe-based pH measurement.

Using an in-house MATLAB script, we were able to extract the ratios of I_{1572}/I_{1606} from the SERS data, and then convert them into pH distribution maps (Figure 6c and 6e) based on the calibration curve plotted in Figure 5b. First, we found that the pH values were consistent no matter whether XY mapping (5.2 ± 0.1) or depth mapping (5.0 ± 0.1) was used (Figure 6f). Furthermore, we compared the average pH values among different cells using surface scans (Figure S8). The internal pH ranged from 4.8 to 5.5, with an average of 5.2. Our results are in good agreement with those reported previously.[26,59] In addition, the SERS spectral peaks of the internalized nanoprobes are free from interferences by cell components or culture medium. A representative SERS spectrum collected from nanoprobes in cancer cells is provided in Figure S9. As discussed above, our 4-Mpy-labelled nanoprobes have strong SERS activity, high pH sensitivity, and low

interference by halide ions due to the functionalization by Br^-. Previous studies also used 4-Mpy as a pH reporter to functionalize nanoprobes, but did not consider the influence of halide ions on the SERS signals of their nanoprobes.[18–21] For example, Shen *et al.* used HCl to adjust the pH of their standards in an attempt to build a calibration curve between pH and the SERS peak ratio of 4-Mpy.[19] The introduction of different amounts of HCl into the standards could alter 4-Mpy relationship with pH, which makes it inaccurate to quantify pH in an unknown sample. Another potential interfering source may come from the cell culture medium, which contains varying concentrations of chloride ions depending on the cell culture medium types. This makes it challenging to quantify pH in biological systems as chloride ions are ubiquitous in such systems. In this study, we resolved this issue by developing a new type of nanoprobe that is resistant to halide ion effects.

Conclusions

This study focuses on the development of reliable nanoprobes for pH quantification in confined microenvironments. We found that nanoprobes modified with 4-Mpy alone are not sensitive to acidic pH unless halide ions exist in the system. Therefore, we proposed the idea to label AuNP surface with Br^-. The labelling enables the following improvements: 1) the pH sensitivity of the 4-Mpy-functionalized nanoprobes was increased, especially in acidic conditions; 2) the high affinity of Br^- towards gold surface reduced the interference of major halide ions (Cl^- and Br^-) on pH measurement; and 3) the Au-Br-4-Mpy complexes formed on the surface of nanoprobes enhanced their SERS activity. With these improvements, the nanoprobes were able to monitor the pH distribution pattern inside individual cancer cells consistently and stably. As many reactions in cancer cells are pH-dependent,[4,5] the nanoprobes we developed provide a reliable tool to advance our knowledge on pH-associated biochemical reactions. For example, it has been

reported that the viability of cancer cells could be inhibited by acidity-reducing drugs, suggesting that controlling cell pH may be a therapeutic strategy for cancer treatment.[4] To further explore this, accurate pH measurement approaches are required. This study fits such need by developing SERS-based nanoprobes that can detect pH sensitively in confined microenvironments of cancer cells with little interference. The application scope of our nanoprobes is expected to be extended to other microenvironments that cannot be reached readily by traditional methods, such as aerosol droplets, soil pore water, and plant tissues.

Acknowledgements

Funding for this work was provided by the National Institutes of Health (NIH) through the NIH Director's New Innovator Award Program (1-DP2-A1112243) to L.M. and through US National Science Foundation grant CBET-1705653 to P.V. and L.M.

References

(1) Haynes, C. L.; McFarland, A. D.; Van Duyne, R. P. Surface-enhanced Raman spectroscopy. *Anal. Chem.* **2005**, *77*, 338a–346a.

(2) Halvorson, R. A.; Vikesland, P. J. Surface-Enhanced Raman Spectroscopy (SERS) for Environmental Analyses. *Environ. Sci. Technol.* **2010**, *44* (20), 7749–7755.

(3) Guo, H.; He, L.; Xing, B. Applications of surface-enhanced Raman spectroscopy in the analysis of nanoparticles in the environment. *Environ. Sci. Nano* **2017**, *4*, 2093–2107.

(4) Fais, S.; Venturi, G.; Gatenby, B. Microenvironmental acidosis in carcinogenesis and

metastases: new strategies in prevention and therapy. *Cancer Metastasis Rev.* **2014**, *33* (4), 1095–1108.

(5) Swietach, P.; Vaughan-Jones, R. D.; Harris, A. L.; Hulikova, A. The chemistry, physiology and pathology of pH in cancer. *Philos. Trans. R. Soc. B Biol. Sci.* **2014**, *369* (1638).

(6) Lyssiotis, C. A.; Kimmelman, A. C. Metabolic Interactions in the Tumor Microenvironment. *Trends Cell Biol.* **2017**, *27* (11), 863–875.

(7) Parolini, I.; Federici, C.; Raggi, C.; Lugini, L.; Palleschi, S.; De Milito, A.; Coscia, C.; Iessi, E.; Logozzi, M.; Molinari, A.; et al. Microenvironmental pH is a key factor for exosome traffic in tumor cells. *J. Biol. Chem.* **2009**, *284* (49), 34211–34222.

(8) Freedman, M. A.; Ott, E. J. E.; Marak, K. E. Role of pH in Aerosol Processes and Measurement Challenges. *J. Phys. Chem. A* **2019**, *123* (7), 1275–1284.

(9) Losey, D. J.; Parker, R. G.; Freedman, M. A. PH Dependence of Liquid-Liquid Phase Separation in Organic Aerosol. *J. Phys. Chem. Lett.* **2016**, *7* (19), 3861–3865.

(10) Williams, A.; Flynn, K. J.; Xia, Z.; Dunstan, P. R. Multivariate spectral analysis of pH SERS probes for improved sensing capabilities. *J. Raman Spectrosc.* **2016**, *47* (7), 819–827.

(11) Wang, F.; Widejko, R. G.; Yang, Z.; Nguyen, K. T.; Chen, H.; Fernando, L. P.; Christensen, K. A.; Anker, J. N. Surface-enhanced Raman scattering detection of pH with silica-encapsulated 4-mercaptobenzoic acid-functionalized silver nanoparticles. *Anal. Chem.* **2012**, *84* (18), 8013–8019.

(12) Wang, Z.; Bonoiu, A.; Samoc, M.; Cui, Y.; Prasad, P. N. Biological pH sensing based on

surface enhanced Raman scattering through a 2-aminothiophenol-silver probe. *Biosens. Bioelectron.* **2008**, *23* (6), 886–891.

(13) Zong, S.; Wang, Z.; Yang, J.; Cui, Y. Intracellular pH sensing using p-aminothiophenol functionalized gold nanorods with low cytotoxicity. *Anal. Chem.* **2011**, *83* (11), 4178–4183.

(14) Liu, Y.; Yuan, H.; Fales, A. M.; Vo-Dinh, T. PH-sensing nanostar probe using surface-enhanced Raman scattering (SERS): Theoretical and experimental studies. *J. Raman Spectrosc.* **2013**, *44* (7), 980–986.

(15) Wei, H.; Willner, M. R.; Marr, L. C.; Vikesland, P. J. Highly stable SERS pH nanoprobes produced by co-solvent controlled AuNP aggregation. *Analyst* **2016**, *141*, 5159–5169.

(16) Jamieson, L. E.; Jaworska, A.; Jiang, J.; Baranska, M.; Harrison, D. J.; Campbell, C. J. Simultaneous intracellular redox potential and pH measurements in live cells using SERS nanosensors. *Analyst* **2015**, *140* (7), 2330–2335.

(17) Capocefalo, A.; Mammucari, D.; Brasili, F.; Fasolato, C.; Bordi, F.; Postorino, P.; Domenici, F. Exploring the potentiality of a SERS-active pH nano-biosensor. *Front. Chem.* **2019**, *7* (June), 1–11.

(18) Jensen, R. A.; Sherin, J.; Emory, S. R. Single Nanoparticle Based Optical pH Probe. *Appl. Spectrosc.* **2007**, *61* (8), 832–838.

(19) Shen, Y.; Liang, L.; Zhang, S.; Huang, D.; Zhang, J.; Xu, S.; Liang, C.; Xu, W. Organelle-targeting surface-enhanced Raman scattering (SERS) nanosensors for subcellular pH sensing. *Nanoscale* **2018**, *10* (4), 1622–1630.

(20) Zheng, X. S.; Hu, P.; Cui, Y.; Zong, C.; Feng, J. M.; Wang, X.; Ren, B. BSA-coated

nanoparticles for improved SERS-based intracellular pH sensing. *Anal. Chem.* **2014**, *86* (24), 12250–12257.

(21) Bi, L.; Wang, Y.; Yang, Y.; Li, Y.; Mo, S.; Zheng, Q.; Chen, L. Highly Sensitive and Reproducible SERS Sensor for Biological pH Detection Based on a Uniform Gold Nanorod Array Platform. *ACS Appl. Mater. Interfaces* **2018**, *10* (18), 15381–15387.

(22) Huang, Y.; Zhu, H.; Liu, G.; Wu, D.; Ren, B.; Tian, Z. When the Signal Is Not from the Original Molecule To Be Detected: Chemical Transformation of para -Aminothiophenol on Ag during the SERS Measurement. *J. Am. Chem. Soc.* **2010**, *132* (27), 9244–9246.

(23) Jung, H. S.; Kim, K.; Kim, M. S. Raman spectroscopic investigation of the adsorption of 4-mercaptopyridine on a silver-sol surface. *J. Mol. Struct.* **1997**, *407* (2–3), 139–147.

(24) Xiang, S. Q.; Zhang, L.; Gao, S. T.; Zhao, L. Bin. Simulating pH-dependent surface-enhanced Raman spectra by density functional theory calculations. *J. Raman Spectrosc.* **2019**, No. April, 1–9.

(25) Yu, H. Z.; Xia, N.; Liu, Z. F. SERS titration of 4-mercaptopyridine self-assembled monolayers at aqueous buffer/gold interfaces. *Anal. Chem.* **1999**, *71* (7), 1354–1358.

(26) Cai, W.-B.; Tian, Z.-W.; Tian, Z.-Q.; Yao, J.-L.; Ren, B.; She, C.-X. Surface Raman spectroscopic investigation of pyridine adsorption at platinum electrodes—effects of potential and electrolyte. *J. Chem. Soc. Faraday Trans.* **2002**, *94* (20), 3127–3133.

(27) Saito, H. Behaviour of the 1025 cm−1 band of SERS spectra due to pyridine on a silver electrode in aqueous halide media. *J. Raman Spectrosc.* **1993**, *24* (4), 191–197.

(28) Sun, S. C.; Bernard, I.; Birke, R. L.; Lombardi, J. R. The Effect of pH, Chloride Ion and Background Electrolyte Concentration on the SERS of Acidified Pyridine Solutions. *J.*

Electroanal. Chem. **1985**, *196*, 359–374.

(29) Jung, H. S.; Kim, K.; Kim, M. S. Raman spectroscopic investigation of the adsorption of 4-mercaptopyridine on a silver-sol surface. *J. Mol. Struct.* **1997**, *407*, 139–147.

(30) Chang, H.; Hwang, K. C. The behavior of pyridine, pyridinium ion, and pyridinium halide on a silver electrode and their SERS spectra. *J. Am. Chem. Soc.* **1984**, *106* (22), 6586–6592.

(31) Grebel, J. E.; Pignatello, J. J.; Mitch, W. A. Impact of Halide Ions on Natural Organic Matter-Sensitized Photolysis of 17 β -Estradiol in Saline Waters. *Environ. Sci. Technol.* **2012**, *46*, 7128–7134.

(32) Flury, M.; Papritz, A. Bromide in the Natural Environment: Occurrence and Toxicity. *J. Environ. Qual.* **1993**, *22*, 747–758.

(33) Wasileski, S. A.; Weaver, M. J. Electrode Potential-Dependent Anion Chemisorption and Surface Bond Polarization As Assessed by Density Functional Theory. *J. Phys. Chem. B* **2002**, *106*, 4782–4788.

(34) Magnussen, O. M.; Ocko, B. M.; Wang, J. X.; Adzic, R. R. In-Situ X-ray Diffraction and STM Studies of Bromide Adsorption on Au (111) Electrodes. *J. Phys. Chem.* **1996**, *100* (13), 5500–5508.

(35) Magnussen, O. M. Ordered Anion Adlayers on Metal Electrode Surfaces. *Chem. Rev.* **2002**, *102*, 679–725.

(36) Zhang, Z.; Li, H.; Zhang, F.; Wu, Y.; Guo, Z.; Zhou, L.; Li, J. Investigation of Halide-Induced Aggregation of Au Nanoparticles into Spongelike Gold. *Langmuir* **2014**, *30*, 2648–2659.

(37) Frens, G. Controlled Nucleation for the Regulation of the Particle Size in Monodisperse Gold Suspensions. *Nat. Phys. Sci.* **1973**, *241* (105), 20–22.

(38) Yuan, H.; Khoury, C. G.; Hwang, H.; Wilson, C. M.; Grant, G. A.; Vo-Dinh, T. Gold nanostars: surfactant-free synthesis, 3D modelling, and two-photon photoluminescence imaging. *Nanotechnology* **2012**, *23* (7), 075102.

(39) Wei, H.; Leng, W.; Song, J.; Liu, C.; Willner, M. R.; Huang, Q.; Zhou, W.; Vikesland, P. J. Real-Time Monitoring of Ligand Exchange Kinetics on Gold Nanoparticle Surfaces Enabled by Hot Spot-Normalized Surface-Enhanced Raman Scattering. *Environ. Sci. Technol.* **2018**, *53*, 575–585.

(40) Lawson, L. S.; Chan, J. W.; Huser, T. A highly sensitive nanoscale pH-sensor using Au nanoparticles linked by a multifunctional Raman-active reporter molecule. *Nanoscale* **2014**, *6* (14), 7971–7980.

(41) Albert, A.; Barlin, G. B. Ionization constants of heterocyclic substances. Part III. Mercapto-derivatives of pyridine, quinoline, and isoquinoline. *J. Chem. Soc.* **1959**, No. 0, 2384–2396.

(42) Kneipp, K.; Kneipp, H.; Manoharan, R.; Hanlon, E. B.; Itzkan, I.; Dasari, R. R.; Feld, M. S. Extremely large enhancement factors in surface-enhanced Raman scattering for molecules on colloidal gold clusters. *Appl. Spectrosc.* **1998**, *52* (12), 1493–1497.

(43) Saute, B.; Narayanan, R. Solution-based direct readout surface enhanced Raman spectroscopic (SERS) detection of ultra-low levels of thiram with dogbone shaped gold nanoparticles. *Analyst* **2011**, *136* (3), 527–532.

(44) Guo, H.; Ruan, F.; Lu, L.; Hu, J.; Pan, J.; Yang, Z.; Ren, B. Correlating the shape, surface

plasmon resonance, and surface-enhanced raman scattering of gold nanorods. *J. Phys. Chem. C* **2009**, *113* (24), 10459–10464.

(45) Bell, S. E. J.; McCourt, M. R. SERS enhancement by aggregated Au colloids: effect of particle size. *Phys. Chem. Chem. Phys.* **2009**, *11* (34), 7455–7462.

(46) Zhang, Y.; Gu, C.; Schwartzberg, A. M.; Chen, S.; Zhang, J. Z. Optical trapping and light-induced agglomeration of gold nanoparticle aggregates. *Phys. Rev. B* **2006**, *73* (16), 165405.

(47) Grant, C. D.; Schwartzberg, A. M.; Norman, T. J.; Zhang, J. Z. Ultrafast Electronic Relaxation and Coherent Vibrational Oscillation of Strongly Coupled Gold Nanoparticle Aggregates. *J. Am. Chem. Soc.* **2003**, *125* (2), 549–553.

(48) Wei, H.; Leng, W.; Song, J.; Willner, M. R.; Marr, L. C.; Zhou, W.; Vikesland, P. J. Improved Quantitative SERS Enabled by Surface Plasmon Enhanced Elastic Light Scattering. *Anal. Chem.* **2018**, *90*, 3227–3237.

(49) Wei, H.; Huang, Q.; Vikesland, P. J. The Aromatic Amine pKa Determines the Affinity for Citrate-Coated Gold Nanoparticles: In Situ Observation via Hot Spot-Normalized Surface-Enhanced Raman Spectroscopy. *Environ. Sci. Technol. Lett.* **2019**, *6*, 199–204.

(50) Otto, A.; Bruckbauer, A.; Chen, Y. X. On the chloride activation in SERS and single molecule SERS. *J. Mol. Struct.* **2003**, *661–662* (1–3), 501–514.

(51) Glaspell, G. P.; Zuo, C.; Jagodzinski, P. W. Surface enhanced raman spectroscopy using silver nanoparticles: The effects of particle size and halide ions on aggregation. *J. Clust. Sci.* **2005**, *16* (1), 39–51.

(52) Kerker, M.; Siiman, O.; Wang, D. S. Effect of aggregates on extinction and surface-

enhanced Raman scattering spectra of colloidal silver. *J. Phys. Chem.* **1984**, *88* (15), 3168–3170.

(53) Li, Y. S.; Cheng, J.; Wang, Y. Surface-enhanced Raman spectra of dyes and organic acids in silver solutions: Chloride ion effect. *Spectrochim. Acta - Part A Mol. Biomol. Spectrosc.* **2000**, *56* (11), 2067–2072.

(54) Jeanmaire, D. L.; Van Duyne, R. P. Surface raman spectroelectrochemistry. *J. Electroanal. Chem. Interfacial Electrochem.* **1977**, *84* (1), 1–20.

(55) Hu, J.; Zhao, B.; Xu, W.; Li, B.; Fan, Y. Surface-enhanced Raman spectroscopy study on the structure changes of 4-mercaptopyridine adsorbed on silver substrates and silver colloids. *Spectrochim. Acta - Part A Mol. Biomol. Spectrosc.* **2002**, *58* (13), 2827–2834.

(56) Do, W. H.; Lee, C. J.; Kim, D. Y.; Jung, M. J. Adsorption of 2-mercaptopyridine and 4-mercaptopyridine on a silver surfaces investigated by SERS spectroscopy. *J. Ind. Eng. Chem.* **2012**, *18* (6), 2141–2146.

(57) Gregório, A. C.; Fonseca, N. A.; Moura, V.; Lacerda, M.; Figueiredo, P.; Simões, S.; Dias, S.; Moreira, J. N. Inoculated cell density as a determinant factor of the growth dynamics and metastatic efficiency of a breast cancer murine model. *PLoS One* **2016**, *11* (11), 1–19.

(58) Pulaski, B. A.; Ostrand-Rosenberg, S. Mouse 4T1 Breast Tumor Model. In *Current Protocols in Immunology*; John Wiley & Sons, Inc.: Hoboken, NJ, USA, 2001; pp 1–16.

(59) Chen, W. L.; Li, F.; Tang, Y.; Yang, S. Di; Li, J. Z.; Yuan, Z. Q.; Liu, Y.; Zhou, X. F.; Liu, C.; Zhang, X. N. Stepwise pH-responsive nanoparticles for enhanced cellular uptake and on-demand intracellular release of doxorubicin. *Int. J. Nanomedicine* **2017**, *12*, 4241–

4256.

Figures

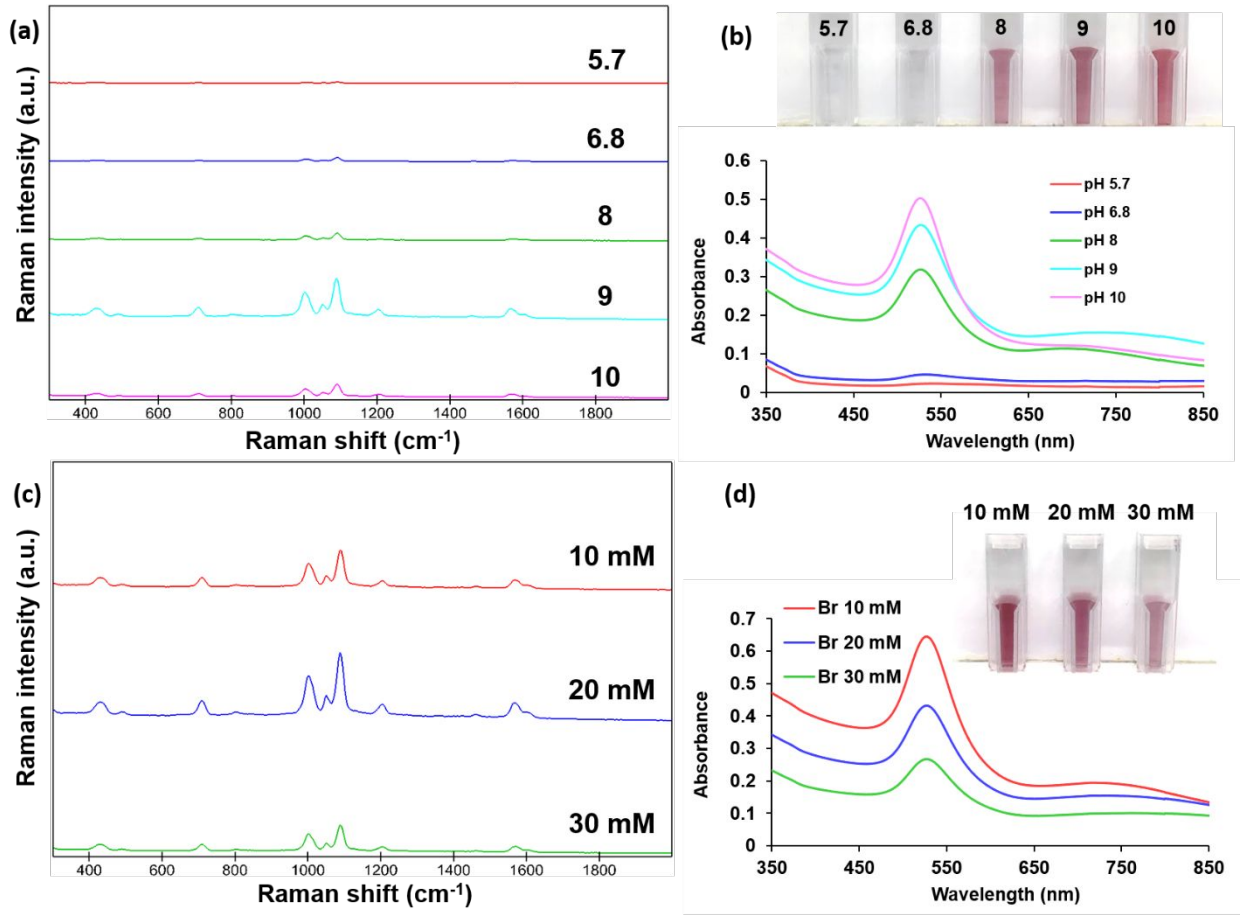

Figure 1. Optimization of pH (a, b) and Br^- concentration (c, d) for nanoprobe synthesis based on SERS spectra (a, c) and UV-Vis absorbance (b, d). The UV-Vis spectra and corresponding optical images were recorded after 2.5× dilution of the nanoprobe solutions. Nanoprobes in (a) and (b) were synthesized with 0.75 μM 4-Mpy, 20 mM Br^-, and 0.01 μM PEG, and those in (c) and (d) were produced at pH 9 with 0.75 μM 4-Mpy and 0.01 μM PEG. The spectra in (a) and (c) were offset to show the differences clearly.

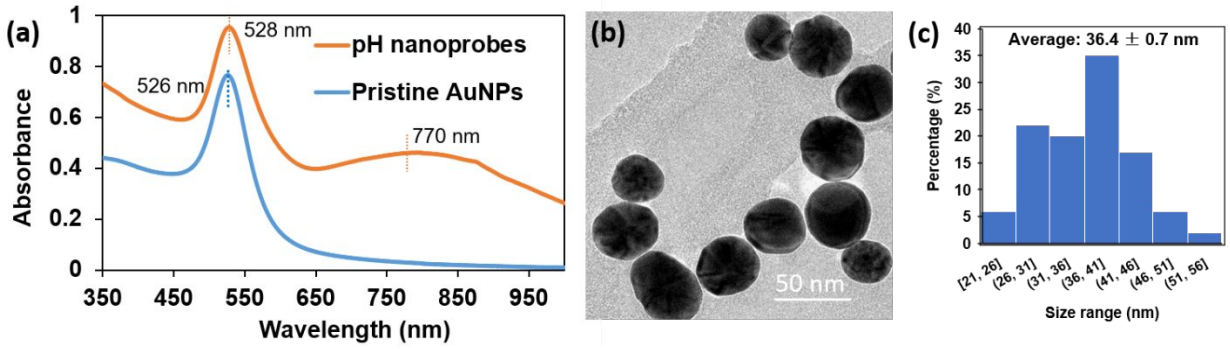

586

587 Figure 2. (a) UV-Vis spectra of the pristine AuNPs and the synthesized pH nanoprobes. (b) TEM

588 image and (c) size distribution of the pristine AuNPs.

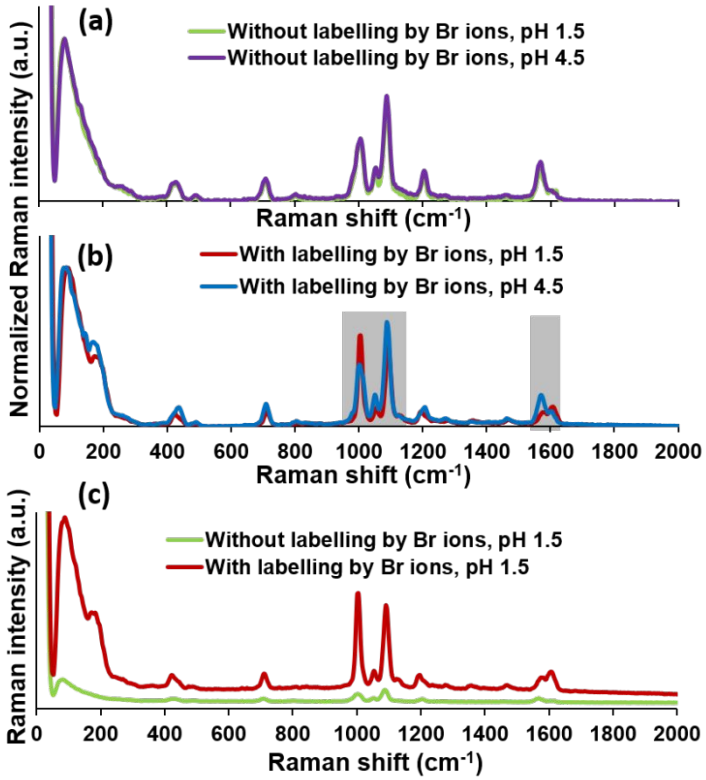

589

590 Figure 3. SERS spectra of nanoprobes without (a) and with (b) labelling by Br^- in H_2SO_4 solutions

591 of pH 1.5 and 4.5. The spectra in (a) and (b) are normalized to the elastic scattering peak at 81 cm^{-1}

592 and these in (c) are the original spectra without normalization.

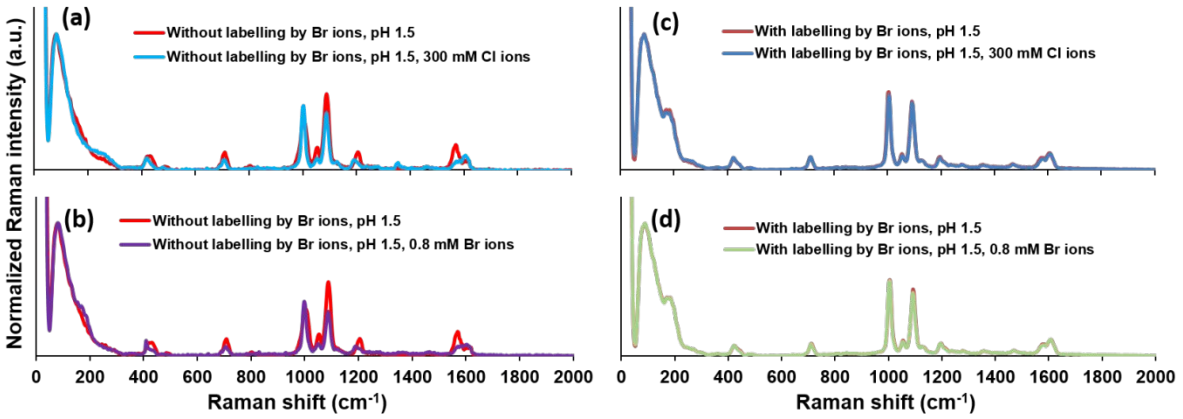

593

594 Figure 4. SERS spectra of nanoprobes labelled without (a, b) and with (c, d) Br^- in H_2SO_4 solution
595 of pH 1.5 that contains Cl^- (a, c) or Br^- (b, d). The spectra were normalized to the elastic scattering
596 peak at 81 cm^{-1}.

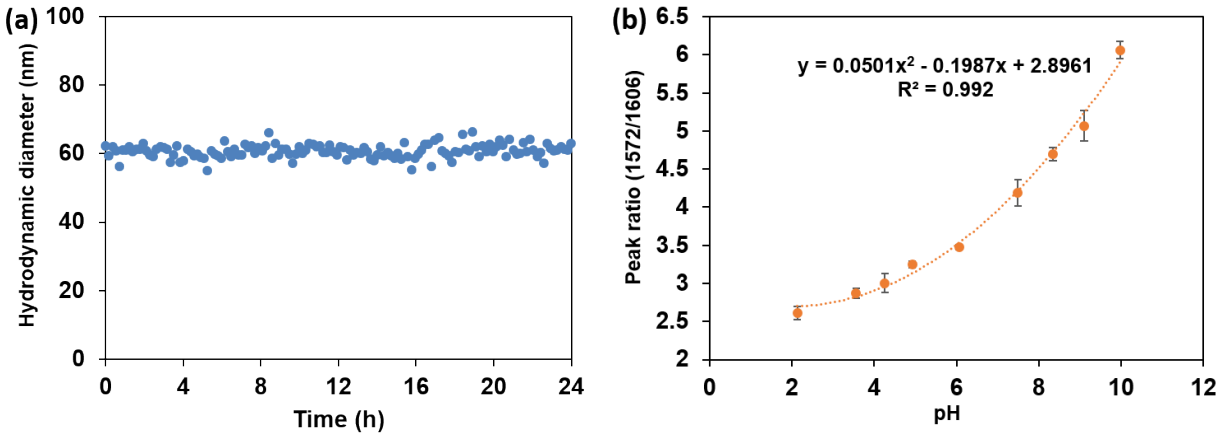

597

598 Figure 5. (a) Hydrodynamic diameter of the pH-sensing nanoprobes in cell culture medium over
599 24 h. (b) Calibration curve based on the nanoprobe SERS peak intensity ratio (I_{1572}/I_{1606}) in cell
600 culture medium of different pHs.

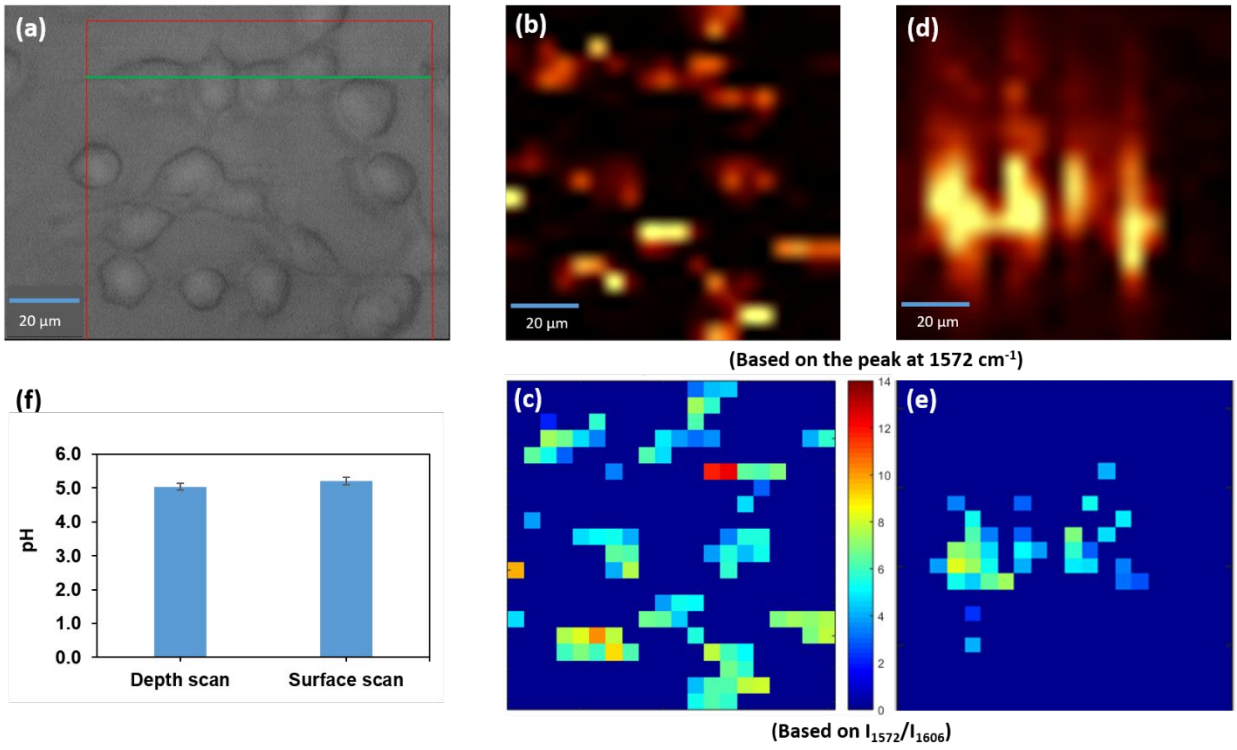

Figure 6. Nanoprobe-enabled pH measurement in 4T1 murine mammary carcinoma cells. (a) Optical microscopy image of 4T1 cancer cells (50× objective); a square area and a line were selected in the optical image for SERS surface mapping and in-depth mapping, respectively. The corresponding maps are shown in (b) and (d) based on the peak intensity at 1572 cm^{-1}. The surface and in-depth pH maps (c and e) were obtained based on the peak intensity ratio of I_{1572}/I_{1606}. The averaged pHs based on surface scan and depth scan are illustrated in panel (f).

Graphical abstract